

Supplementary Information

Ultrasound Synthesis of Lead Halide Perovskite Nanocrystals

Dong Myung Jang,[†] Duk Hwan Kim,[†] Kidong Park,[†] Jeunghye Park,^{*,†} Jong Woon Lee,[‡] and Jae Kyu Song[‡]

[†]Department of Chemistry, Korea University, Jochiwon 339-700, Korea

[‡]Department of Chemistry, Kyung Hee University, Seoul 130-701, Korea

* Corresponding Author: parkjh@korea.ac.kr

Contents

I. Experimental Details: Material and Methods

II. Supporting Tables

Table S1. Bandgap of perovskite NCs

Table S2. Summary of previous works on perovskite photodetectors.

Table S3. Fitted parameters of the decay curve of the PL for APbX₃ NCs.

Table S4. Fitted parameters of the decay curve of the PL for APbX₃ mixed halide NCs.

III. Supporting Figures

Figure S1. XRD pattern of APbX₃ NCs.

Figure S2. HRTEM images of APbX₃ NCs.

Figure S3. EDX spectra of APbX₃ NCs.

Figure S4. Photographs showing the ultrasound induced synthesis of APbX₃ NCs.

Figure S5. HRTEM images of MAPbBr₃ NCs as a function of irradiation time.

Figure S6. PL spectra of MAPbBr₃ NCs, synthesized using different ligand condition.

Figure S7. Photographs showing the solubility of reactants and products in toluene.

Figure S8. Quantum yields of APbX₃ NCs.

Figure S9. PL spectra of $\text{MAPbBr}_{3-x}\text{Cl}_x$ and $\text{MAPbBr}_{3-x}\text{I}_x$ NCs and their band gaps.

Figure S10. XRD pattern of (a) $\text{MAPbBr}_{3-x}\text{Cl}_x$ and $\text{MAPbBr}_{3-x}\text{I}_x$, and (b) $\text{CsPbBr}_{3-x}\text{Cl}_x$ and $\text{CsPbBr}_{3-x}\text{I}_x$ NCs.

Figure S11. Time-resolved PL spectrum data of APbX_3 NCs.

Figure S12. Atomic-force microscopy image of MAPbBr_3 NC films.

Figure S13. Time-resolved PL spectrum data of APbX_3 mixed halide NCs.

Figure S14. Photocurrent of $\text{CsPbBr}_{3-x}\text{I}_x$ NC films.

IV. References

I. Experimental Details: Materials and Methods

Materials. Commercially available PbCl_2 powder (Aldrich), PbBr_2 powder (Aldrich), PbI_2 powder (Aldrich), aqueous HCl (36 wt% in water, Aldrich), aqueous HBr (48 wt% in water, Aldrich), aqueous HI (57 wt% in water, Aldrich), CH_3NH_2 /methanol solution (40 wt%, TCI), $\text{HN}=\text{CHNH}_2\cdot\text{CH}_3\text{COOH}$ powder (formamidinium acetate salt, Aldrich), CsCl powder (Aldrich), CsBr powder (Aldrich), CsI powder (Aldrich), and $\text{CH}_3(\text{CH}_2)_7\text{CH}=\text{CH}(\text{CH}_2)_7\text{CH}_2\text{NH}_2$ (oleylamine; Aldrich, 70%) were used without further purification.

Preparation of organic ammonium halides. Organic ammonium halides $\text{CH}_3\text{NH}_3\text{X}$ (MAX) and $\text{HN}=\text{CHNH}_3\text{X}$ (or $\text{HC}(\text{NH}_2)_2\text{X}$, FAX), where $\text{X} = \text{Cl}$, Br , and I , were prepared as precursors for the APbX_3 NCs. In order to synthesize MABr and FABr, 0.27 mol CH_3NH_2 (23 mL) or 28.1 mg $\text{HN}=\text{CHNH}_2\cdot\text{CH}_3\text{COOH}$ was mixed with 0.23 mol HBr (26 mL), respectively, and stirred for 2 h by keeping the temperature of reaction vessel (100 mL) at 0 °C using an ice bath. After the reaction, the mixture was evaporated at 50–60 °C (using an oil bath), followed by crystallization. HI (30 mL) was used instead of HBr to prepare MAI and FAI, while HCl (23 mL) was used to prepare MACl and FACl. In all cases, the precipitate was washed several times with diethyl ether and then dried under vacuum.

Synthesis of MAPbX_3 , CsPbX_3 , and FAPbX_3 NCs. For the synthesis of APbX_3 NCs, 0.1 mmol PbX_2 , 0.1 mmol MAX (or FAX, CsX), and 0.3 mmol (0.1 mL) oleylamine (OAm) were added to toluene (10 mL) to form a precursor solution. The reaction vessel (50 mL) of the precursor solution was positioned in a high-density probe-type ultrasonicator (Q700, QSonica; 20 kHz, maximum power output of 700 W). The temperature inside the reaction vessel was monitored using thermocouple wires and

maintained at 20 °C by immersing it in a water jacket connected to a circulator with a temperature controller. The sonication tip was pulsed for 10 s on and 2 s off to avoid excessive heating. After ultrasonic irradiation for 10 min to 3 h, the precipitates were collected by centrifugation at 7000 rpm for 10 min. Finally, the nanocrystals were washed with toluene.

Characterization. The structure of products were analyzed by field-emission transmission electron microscopy (TEM, Jeol JEM 2100F and FEI TECNAI G² 200 kV), and high-voltage TEM (HVEM, Jeol JEM ARM 1300S, 1.25 MV). To identify the compositions of the materials, scanning transmission electron microscopy (STEM), selected area electron diffraction (SAED), and energy-dispersive X-ray fluorescence spectroscopy (EDX) with elemental maps were acquired using TEM (FEI Talos F200X) operated at 200 keV equipped with a high-brightness Schottky field emission electron source (X-FEG) and Super-X EDS detector system (Bruker Super-X). X-ray diffraction (XRD) pattern measurements were carried out in a Rigaku D/MAX-2500 V/PC using Cu K_α radiation ($\lambda = 1.54056 \text{ \AA}$). High-resolution X-ray diffraction (XRD) patterns were also obtained using the 9B and 3D beam lines of the Pohang Light Source (PLS) with monochromatic radiation ($\lambda=1.54595 \text{ \AA}$).

Steady-state photoluminescence spectrum of the samples was measured using a He-Cd laser (325 nm). For steady-state and time-resolved photoluminescence studies, samples were excited by the second harmonic (355 nm, 400 nm) or fundamental (710 nm) of a cavity-dumped oscillator (Mira/PulseSwitch, Coherent, 31.25 kHz, 150 fs). Emission was collected using the focusing lens, spectrally resolved using a monochromator (Sciencetech 9055), detected using a photomultiplier (PMA-182-P-M, PicoQuant), and recorded using a time-correlated single photon counter (PicoHarp300, PicoQuant).

Quantum yield measurement. The relative quantum yield of APbX₃ NCs was determined using a well-known comparative method.^{S1} The integrated fluorescence intensity and absorbance of the perovskite NC/toluene solution (or suspension) at different concentrations were measured with an excitation wavelength of 325 nm. The gradient of the graph is then compared with a standard Rhodamine 6G (99%, Aldrich) ethanol solution was chosen as the standard since it has a known quantum yield of 100%. We can obtain quantum yield by equation: $\Phi_X = \Phi_{ST} (G_X/G_{ST}) (\eta_X^2/\eta_{ST}^2)$, where X in the equation denotes the test (APbX₃/toluene solution) sample and ST denotes the standard (Rhodamine 6G/ethanol solution) sample. The Φ , G, and η in the equation denote the quantum yield, the slope of the integrated fluorescence intensity *versus* absorbance, and the refractive index of the solvent ($\eta_{\text{toluene}}=1.497$ and $\eta_{\text{ethanol}}=1.361$), respectively.

Photocurrent Measurement. The Ti (20 nm)/Au (80 nm) electrode structure was deposited onto a 1 μm thick SiO_x layered Si substrate by photolithography using a patterned mask. The gap between the electrodes was 2 μm . A spin coater was used to deposit the NCs (dispersed in toluene) as a film between the electrodes. The film thickness was controlled to be 3 μm . We tested the devices on a probe station with parametric test equipment (Agilent E5270A) at room temperature. A light-emitting diode (Mightex System LEDs, 365 nm, 150 mW) was used as the light source.

II. Supporting Tables

Table S1. Band gap of colloidal perovskite NCs, reported in the previous works.

Sample		Band gap (eV)	References
MAPbCl ₃	10 nm size NCs	3.05	Present work
	Powder	3.00	S2
	Single crystals	3.05	S3
MAPbBr ₃	10 nm size NCs	2.33	Present work
	Powder	2.20	S2
	Single crystal	2.3	S3
	Single crystal	2.21	S4
MAPbI ₃	10 nm size NCs	1.64	Present work
	Powder	1.53	S2
	Single crystal	1.51	S4
	Films	1.57	S5
CsPbCl ₃	10 nm size NCs	3.18	Present work
	9 nm size NCs	3.18	S6
	Film	3.04	S7
CsPbBr ₃	10 nm size NCs	2.43	Present work
	9 nm size NCs	2.43	S6
	Single crystal	2.25	S8
CsPbI ₃	10 nm size NCs	1.88	Present work
	9 nm size NCs	1.87	S6
	Film	1.73	S5
FAPbCl ₃	10 nm size NCs	3.00	Present work
FAPbBr ₃	10 nm size NCs	2.29	Present work
	Film	2.26	S9, S10
	NC Film	2.14	S11
FAPbI ₃	10 nm size NCs	1.54	Present work
	Film	1.48	S5
	Film	1.47	S12

Table S2. Summary of characteristics of previous MAPbI₃, MAPbBr₃, MAPbCl₃ polycrystalline or NC photodetectors.

Ref.	Devices	λ (nm) ^a	Light Intensity	I _p ^b	S ^c	R (AW ⁻¹) ^d	G ^e	D* ^f
S13	ITO/SEDOT:PSS/ MAPbI _{3-x} Cl _x /PCBM/PFN/Al	550	1 mWcm ⁻²	~10 ⁻³ Acm ⁻² at 0.1 V				8×10 ¹³
S14	MAPbI ₃ nanowire film	633 (laser)	6.78 μW	40 nA at 1.0 kV/cm	--	5×10 ⁻³		
S15	MAPbI ₃ Film	365	0.21 mWcm ⁻²	0.8 μA at 3 V	--	3.49	1.19×10 ³	10 ⁹
S16	MAPbI ₃ /TiO ₂	AM1.5 (100 mWcm ⁻²)	0.5 mWcm ⁻²	9.75 nA at 3 V	--	0.49×10 ⁻⁶		
S17	MAPbI ₃ /graphene	520 (laser)	1 μW	0.18 mA at 0.1 V	--	180	5×10 ⁴	10 ⁹
S18	ITO/MAPbI ₃ /MoO ₃ /Ag	532 (laser)	0.2 mWcm ⁻²	~10 ³ mA at -0.1 V	--	203	475	
S19	ITO/MAPbI ₃ /PCBM/C ₆₀ /Al	White	143 mWcm ⁻²	0.1 Acm ⁻² at 1.5 V		0.21		7.4×10 ¹² (at 680 nm)
S20	MAPbBr ₃ Nanowires film	420	27.5 mWcm ⁻²	4 nA at 2 V	61.9			
S21	MAPbI ₃ Nanowires film	650	100 μWcm ⁻²	20 nA at 10 V	300	0.10	10 ⁴	1.02×10 ¹²
S22	MAPbBr ₃ single crystals	520 (LED)	2 μW	70 μA at 5 V		4000		10 ¹³
S23	MAPbI ₃ /PDPP3T	650	500 μWcm ⁻²	~3 μA at 1 V		25×10 ⁻³		1.5×10 ¹⁰

S24	MAPbCl ₃ Single crystals	385	4 nW	~300 nA at 2.5 V		18	100	10 ¹²
S25	MAPbI ₃ /MoS ₂	520	6 mWcm ⁻²	10 ⁻⁵ A/μm at 5V (with gate = 20 V)		4.9×10 ³		8.76×10 ¹⁰
S26	MAPbI ₃ film	white	0.5 mWcm ⁻²	~3 μA at 1V (at 810 nm)		1640	2509	
S27	CsPbI ₃ NCs	405	1.98 mWcm ⁻²	~0.8 μA at 3V	>10 ⁵			
This work	APbX ₃ NCs (A = Cs, MA; X = Br, I)	365 (LED)	60 mWcm ⁻²	150 nA at 2V	1.5×10 ⁵	0.15×10 ⁻³		

^a Wavelength; ^b Photocurrent; ^c S = Photosensitivity = I_p/I₀, where I_p is photocurrent (A), and I₀ is dark current; ^d R (AW⁻¹) = (Photo) Responsivity = I_p/P, where P = light intensity (W); ^e G = Gain = number of electrons detected per incident photon = R (hv/q);, where hv is photon energy, q is electron charge (1.602×10⁻¹⁹ C); ^f D* (cmHz^{1/2}W⁻¹ = Jones) = (Photo) Detectivity = conversion rate from photons to electrons/holes = (AΔf)^{1/2} R/I₀, where A is effective area of detector and Δf is electrical bandwidth.

Table S3. Fitted parameters of the decay curve of the PL, measured for (a) APbX₃ perovskite NCs in toluene; (b) 3 μm-thick APbX₃ perovskite NC films, using exponential decay function. The average decay time $\langle\tau\rangle$ was calculated using the equation, $\langle\tau\rangle = \sum_i f_i\tau_i$, where f_i is the fraction of component i and τ_i is its decay time.

(a) APbX ₃ perovskite NCs in toluene								
	A	f ₁	τ ₁ (ns)	f ₂	τ ₂ (ns)	f ₃	τ ₃ (ns)	⟨τ⟩ (ns)
APbBr ₃	MA	0.58	7.3	0.41	19.1	0.01	108	13.5
	Cs	0.66	3.7	0.33	11.6	0.01	222	7.4
	FA	0.13	10.4	0.32	68.3	0.55	427	230
APbI ₃	MA	0.58	18.7	0.41	42.5	0.01	199	31.8
	Cs	0.45	8.3	0.55	14.2			12.2
	FA	0.47	5.4	0.32	50.3	0.21	427	100

(b) APbX ₃ perovskite NC films								
	A	f ₁	τ ₁ (ns)	f ₂	τ ₂ (ns)	f ₃	τ ₃ (ns)	⟨τ⟩ (ns)
APbBr ₃	MA	0.55	4.2	0.38	21.9	0.07	148	21.7
	Cs	0.54	2.9	0.40	16.1	0.06	105	14.5
	FA	0.45	4.8	0.41	26.8	0.14	137	32.6
APbI ₃	MA	0.48	7.3	0.36	37.0	0.16	273	60.3
	Cs	0.56	3.1	0.36	15.4	0.08	84.0	13.8
	FA	0.56	3.8	0.32	24.6	0.12	158	30.4

Table S4. Fitted parameters of the decay curve of the PL, measured for (a) APbX₃ MAPbBr_{3-x}Cl_x and MAPbBr_{3-x}I_x; (b) CsPbBr_{3-x}Cl_x and CsPbBr_{3-x}I_x NCs in toluene NCs. The average decay time $\langle\tau\rangle$ was calculated using the equation, $\langle\tau\rangle = \sum_i f_i \tau_i$, where f_i is the fraction (%) of component i and τ_i is its decay time.

(a) Fitted parameters of the PL decay curves, measured for MAPbBr_{3-x}Cl_x and MAPbBr_{3-x}I_x NCs in toluene.

	x	f_1	τ_1 (ns)	f_2	τ_2 (ns)	f_3	τ_3 (ns)	$\langle\tau\rangle$ (ns)
MAPbBr _{3-x} Cl _x	0	0.58	7.32	0.41	19.1	0.01	109	13.5
	1	0.53	5.39	0.46	15.0	0.01	141	10.6
	2	0.52	6.44	0.47	14.5	0.01	160	10.7
	3	0.39	2.39	0.47	10.7	0.14	35.1	10.9
MAPbBr _{3-x} I _x	1	0.30	2.44	0.46	7.7	0.24	16.2	8.1
	2	0.38	9.98	0.60	24.6	0.02	122	20.8
	3	0.58	18.7	0.66	42.5	0.01	199	31.8

(b) Fitted parameters of the PL decay curves, measured for CsPbBr_{3-x}Cl_x and CsPbBr_{3-x}I_x NCs in toluene.

	x	f_1	τ_1 (ns)	f_2	τ_2 (ns)	f_3	τ_3 (ns)	$\langle\tau\rangle$ (ns)
CsPbBr _{3-x} Cl _x	0	0.66	3.7	0.33	11.6	0.01	222	7.4
	1	0.49	1.70	0.40	4.48	0.11	14.5	3.9
	2	0.41	0.62	0.53	3.63	0.06	15.2	3.4
	3	0.70	0.59	0.25	2.63	0.05	13.0	1.8
CsPbBr _{3-x} I _x	1	0.20	2.50	0.69	6.59	0.10	16.3	6.8
	2	0.73	10.4	0.27	20.5	0.13	243	13.7
	3	0.45	8.3	0.55	14.2			12.2

III. Supporting Figures

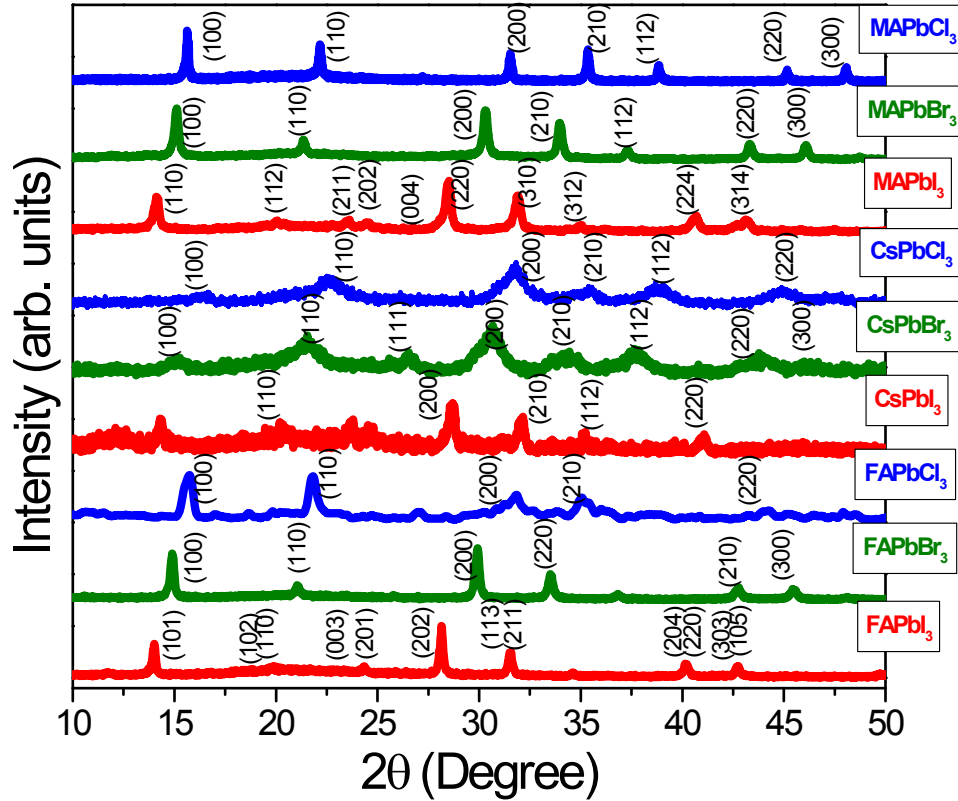


Figure S1. XRD pattern of lead halide perovskite NCs. The peaks of the MAPbCl₃, MAPbBr₃, and MAPbI₃ were indexed using the references: $a = 5.675 \text{ \AA}$ for cubic phase MAPbCl₃; $a = 5.90 \text{ \AA}$ for cubic phase MAPbBr₃; $a = 8.80 \text{ \AA}$ and $c = 12.685 \text{ \AA}$ for tetragonal phase MAPbI₃.^{S28} $a = 5.605 \text{ \AA}$ for cubic phase CsPbCl₃; $a = 5.874 \text{ \AA}$ for cubic phase CsPbBr₃; $a = 6.348 \text{ \AA}$ for cubic phase CsPbI₃.^{S29,S30} In case of FAPbX₃, the observed XRD peaks correspond to cubic phase FAPbCl₃ with $a = 5.68 \text{ \AA}$, cubic phase FAPbBr₃ with $a = 6.00 \text{ \AA}$, and trigonal phase FAPbI₃ with $a = 8.9920 \text{ \AA}$ and $c = 11.0139 \text{ \AA}$, respectively, consistent with previous studies.^{S11,S12}

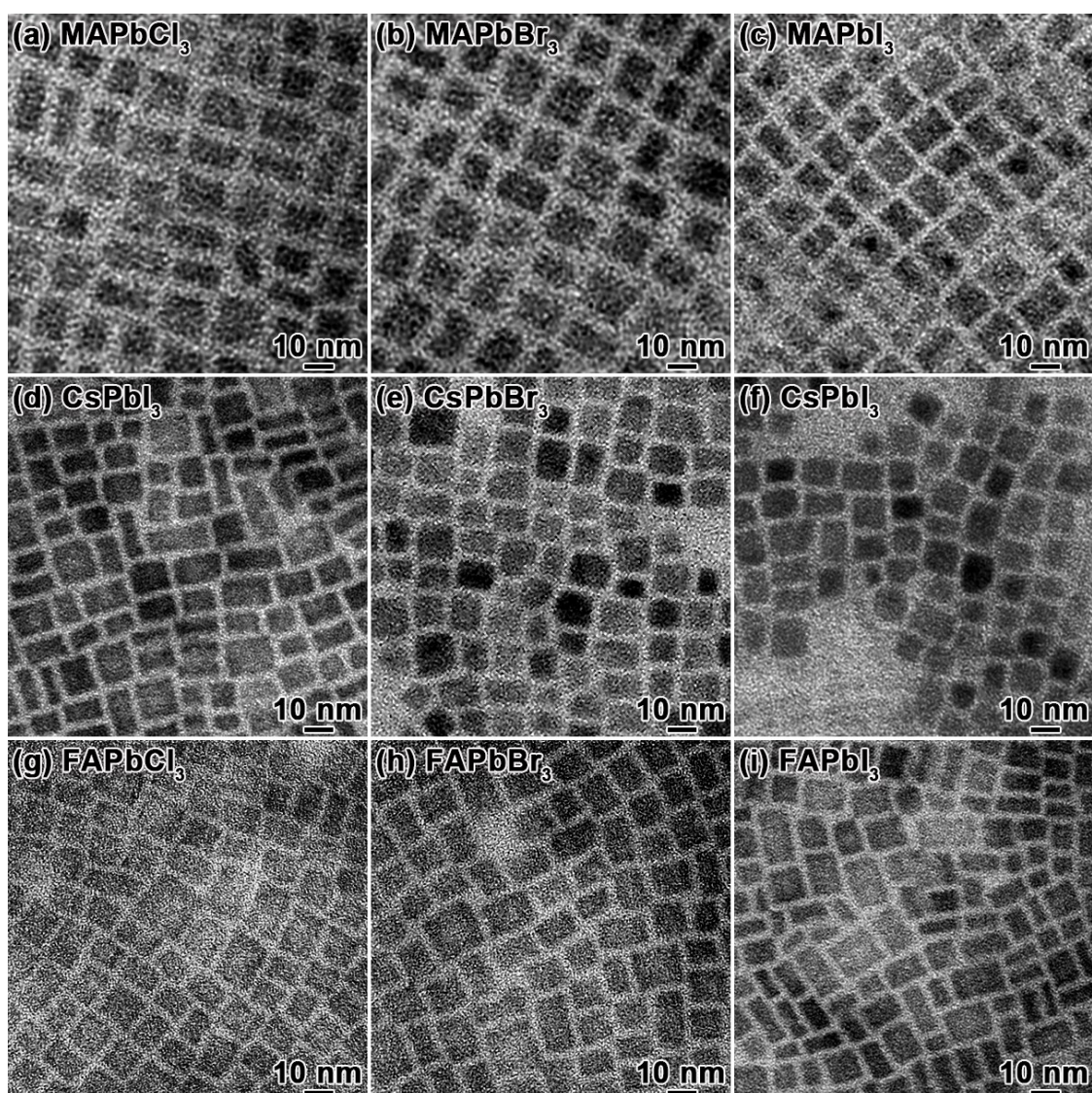


Figure S2. HRTEM images of perovskite NCs; (a) MAPbCl₃, (b) MAPbBr₃, (c) MAPbI₃, (d) CsPbCl₃, (e) CsPbBr₃, (f) CsPbI₃, (g) FAPbCl₃, (h) FAPbBr₃, and (i) FAPbI₃.

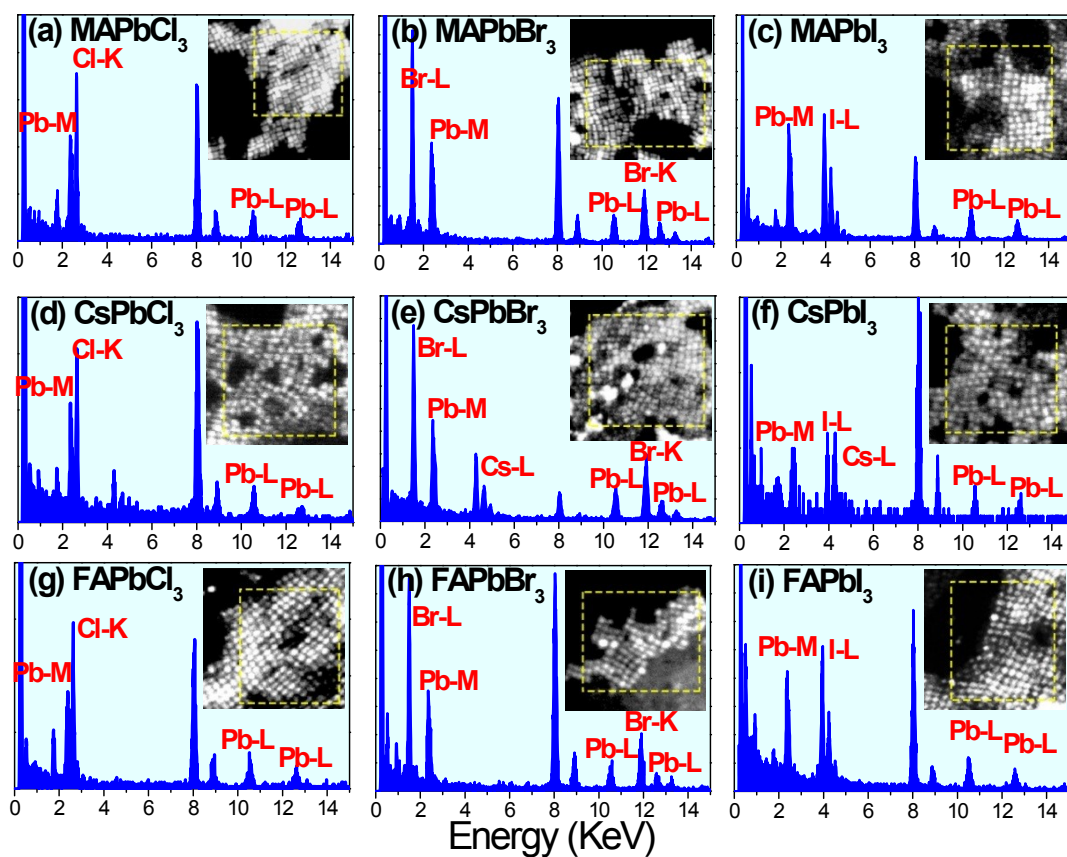


Figure S3. EDX spectra of (a) MAPbCl₃, (b) MAPbBr₃, (c) MAPbI₃, (d) CsPbCl₃, (e) CsPbBr₃, (f) CsPbI₃, (g) FAPbCl₃, (h) FAPbBr₃, and (i) FAPbI₃, with corresponding STEM images. The composition was calculated using Pb L shell, Cl K shell, Br K, I L, and Cs L shell peaks.

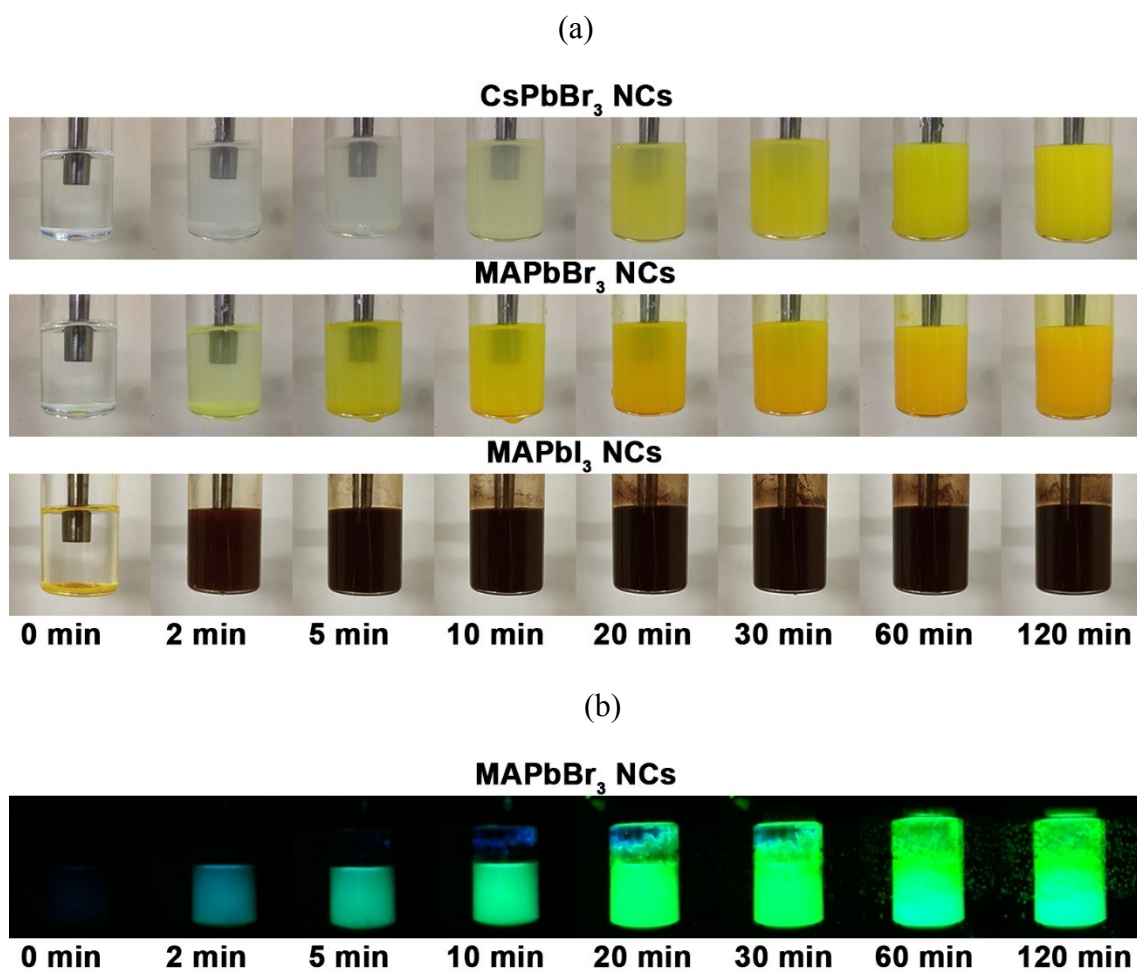


Figure S4. (a) Photographs showing the ultrasound-induced synthesis of perovskite NCs. The precursors dissolved and reacted to produce yellow MAPbBr₃ NCs, yellow CsPbBr₃ NCs, and dark brown MAPbI₃ NCs. (b) Photographs showing the light emitting MAPbBr₃ NCs that were synthesized by ultrasound irradiation of the precursor solution. The intensity of fluorescence increased with time, which can be seen under UV-lamp irradiation.

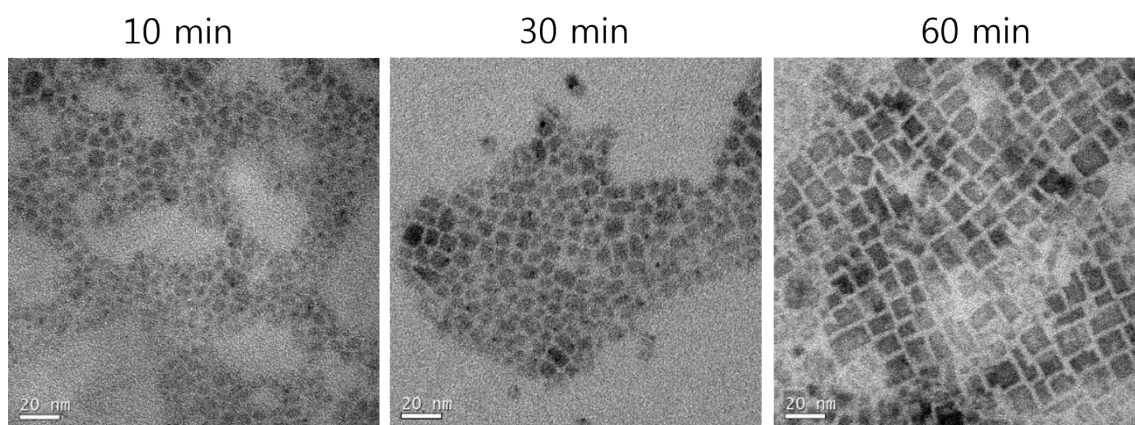


Figure S5. HRTEM images of MAPbBr₃ NCs as a function of irradiation time (10, 30, and 60 min). As the irradiation time increased, the average size increased and a plate-like morphology was formed.

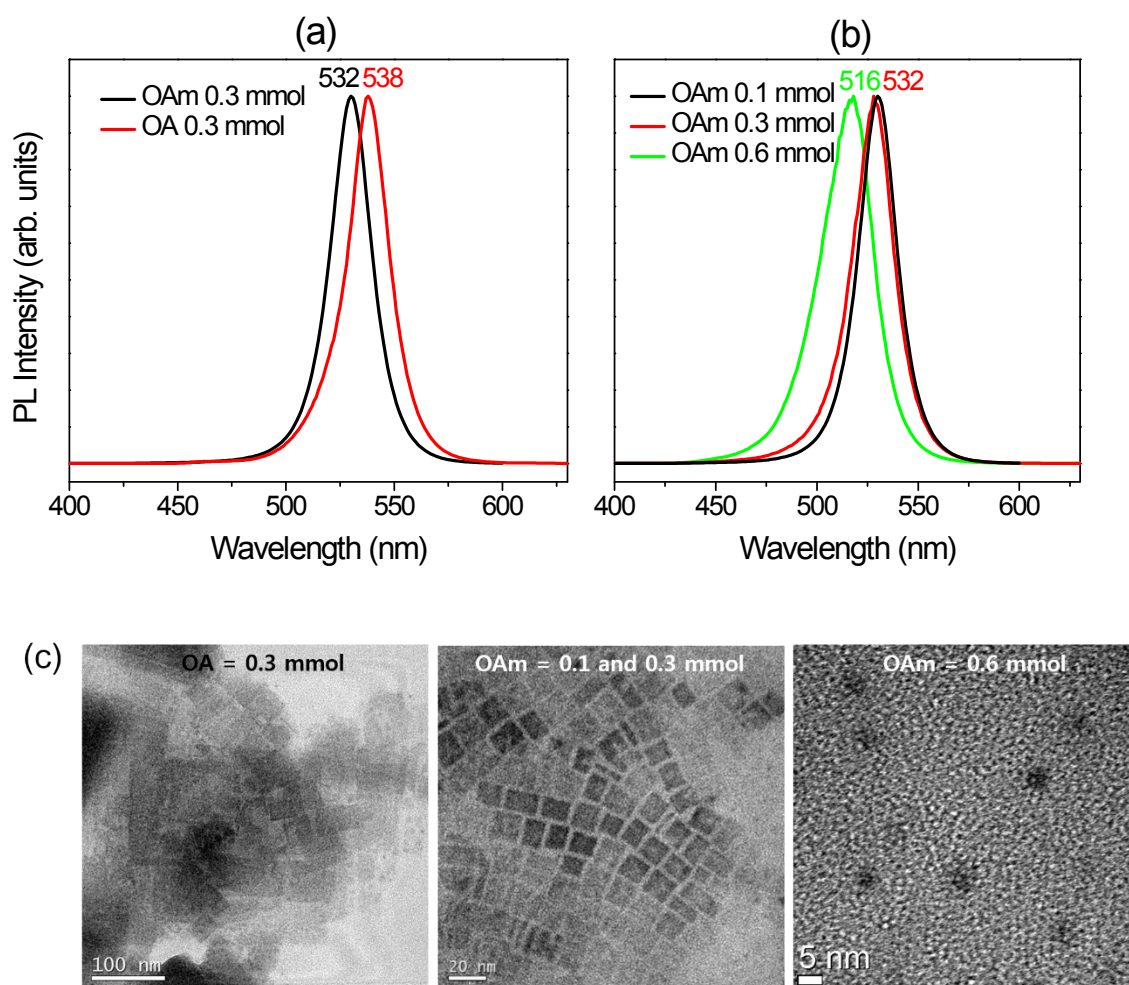


Figure S6. PL spectra of MAPbBr₃ NCs in toluene, synthesized using (a) 0.3 mmol octylamine (OA) and oleylamine (OAm) with a ratio of MAPbBr₃:OA (or OAm) = 1:3, and (b) 0.1, 0.3, and 0.6 mmol OAm; MAPbBr₃:OAm = 1:1, 1:3, and 1:6. (c) TEM images of MAPbBr₃ NCs, synthesized using 0.3 mmol OA (MAPbBr₃:OA = 1:3), 0.1 and 0.3 mmol OAm (MAPbBr₃:OAm = 1:1 or 1:3), and 0.6 mmol OAm (MAPbBr₃:OAm = 1:6).

With 0.3 mmol OA, the PL peak red-shifted from 532 nm (2.33 eV) to 538 nm (2.30 eV), with a broader width compared to that obtained when using 0.3 mmol OAm. The NCs were 20–50 nm when produced using 0.3 mmol OA, while they were 10 nm when 0.3 mmol OAm was used. This result indicates that OAm was a more effective ligand than OA for producing uniform-sized NCs. As the amount of OAm used was increased, the PL peak blue-shifted from 532 nm (2.33 eV) to 516 nm (2.40 eV). The size of the NCs decreased to 5 nm, with a dot morphology being observed.

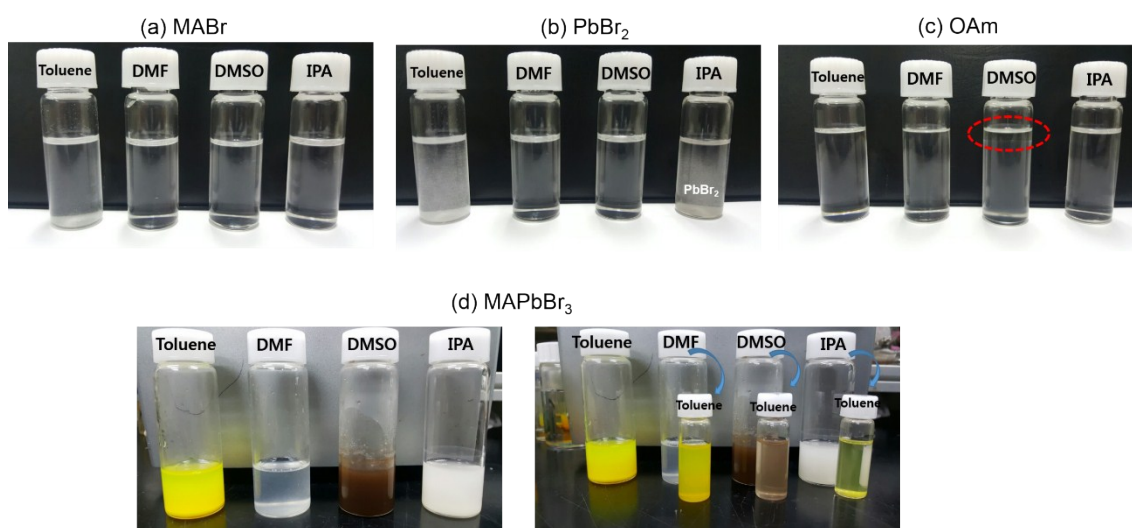


Figure S7. Photographs showing the solubility of (a) MABr, (b) PbBr₂, (c) OAm, and (d) the product (MAPbBr₃) after being sonicated for 2 h in the presence of OAm in toluene, dimethyl formamide (DMF), dimethyl sulfoxide (DMSO), and isopropyl alcohol (IPA).

Both MABr and PbBr₂ were soluble in DMF, so sonication was not necessary to increase the degree of dissolution. DMSO did not mix with OAm (see the separated layers marked by circle). In the case of IPA, the solubility of PbBr₂ was almost negligible compared to that of MABr, and the yield of the perovskite NCs was greatly reduced compared to when using toluene. Toluene mixed with OAm did not dissolve the precursors well, meaning that sonication could significantly affect their solubilities. After 2 h of sonication, colloidal MAPbBr₃ NCs (yellow) were synthesized in toluene. When toluene was added to DMF and IPA samples, MAPbBr₃ NCs precipitated from the solutions, as shown in (d).

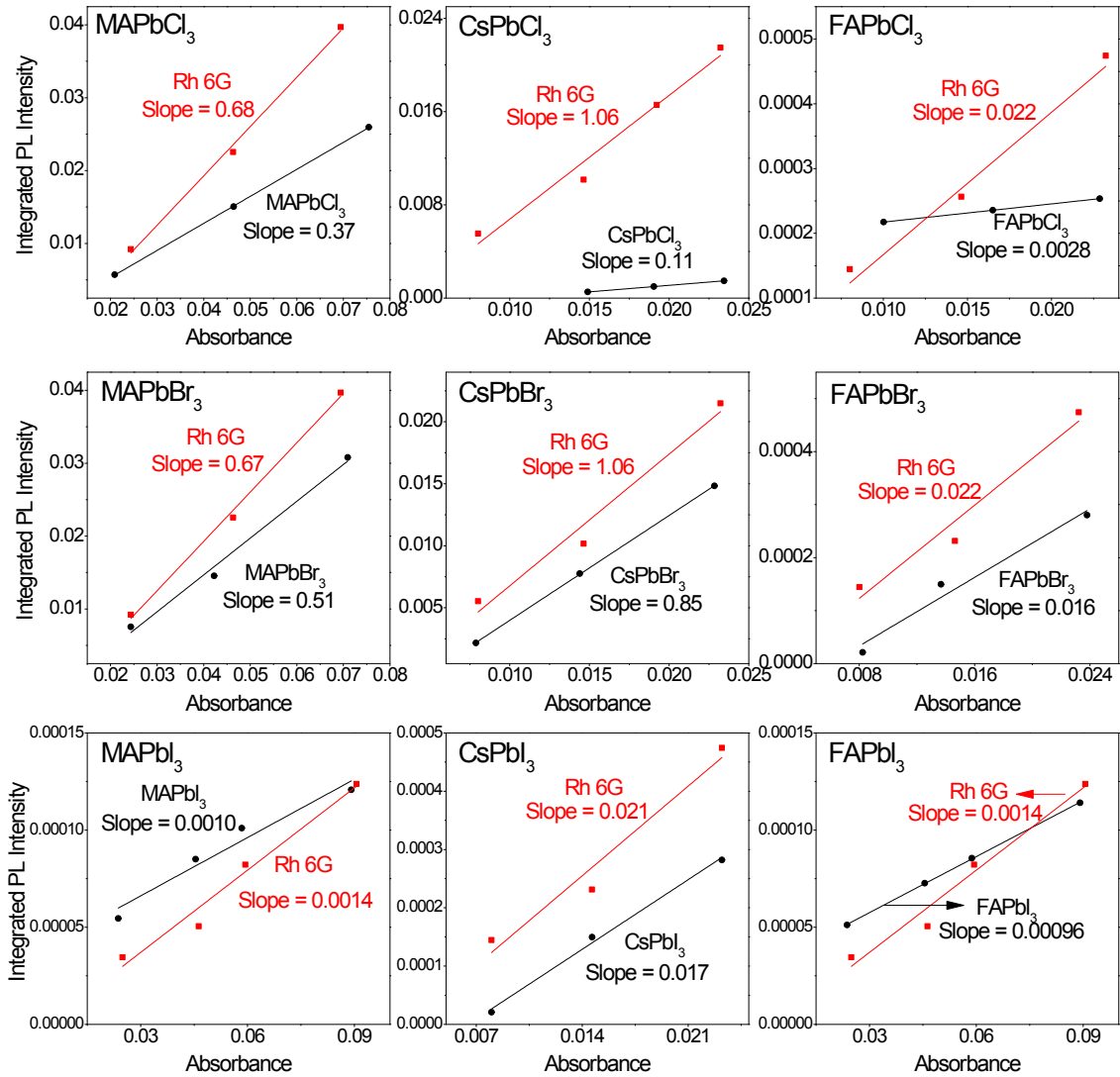


Figure S8. The integrated PL intensity *versus* absorbance of APbX₃/toluene solution, with the corresponding data of Rhodamine 6G (Rh6G)/ethanol solution (reference). The excitation wavelength of was fixed at 325 nm. The quantum yield is calculated by the equation, $\Phi_X = \Phi_{ST} (G_X/G_{ST}) (\eta_X^2/\eta_{ST}^2)$, where X denotes APbX₃/toluene solution sample and ST denotes the standard (Rh6G/ethanol solution) sample.^{S1} We used $\eta_X^2/\eta_{ST}^2 = 1.21$ and $\Phi_{ST} = 95\%$. The quantum yield (Φ) was summarized in the following table. The quantum yield of our NCs was compared with that of the colloidal NCs reported by other

group, showing the comparable value.

	A	G_X/G_{ST}	Φ (%)	Reference value
APbCl ₃	MA	0.54	63	50-70 ^{S28}
	Cs	0.10	12	10 ^{S29}
	FA	0.13	15	--
APbBr ₃	MA	0.76	86	84 (25°C), ^{S30} 83 ^{S31} , 90.5 ^{S32}
	Cs	0.80	92	92 ^{S29}
	FA	0.73	84	85 ^{S33}
APbI ₃	MA	0.71	82	50-70 ^{S28}
	Cs	0.81	89	90 ^{S29}
	FA	0.69	78	--

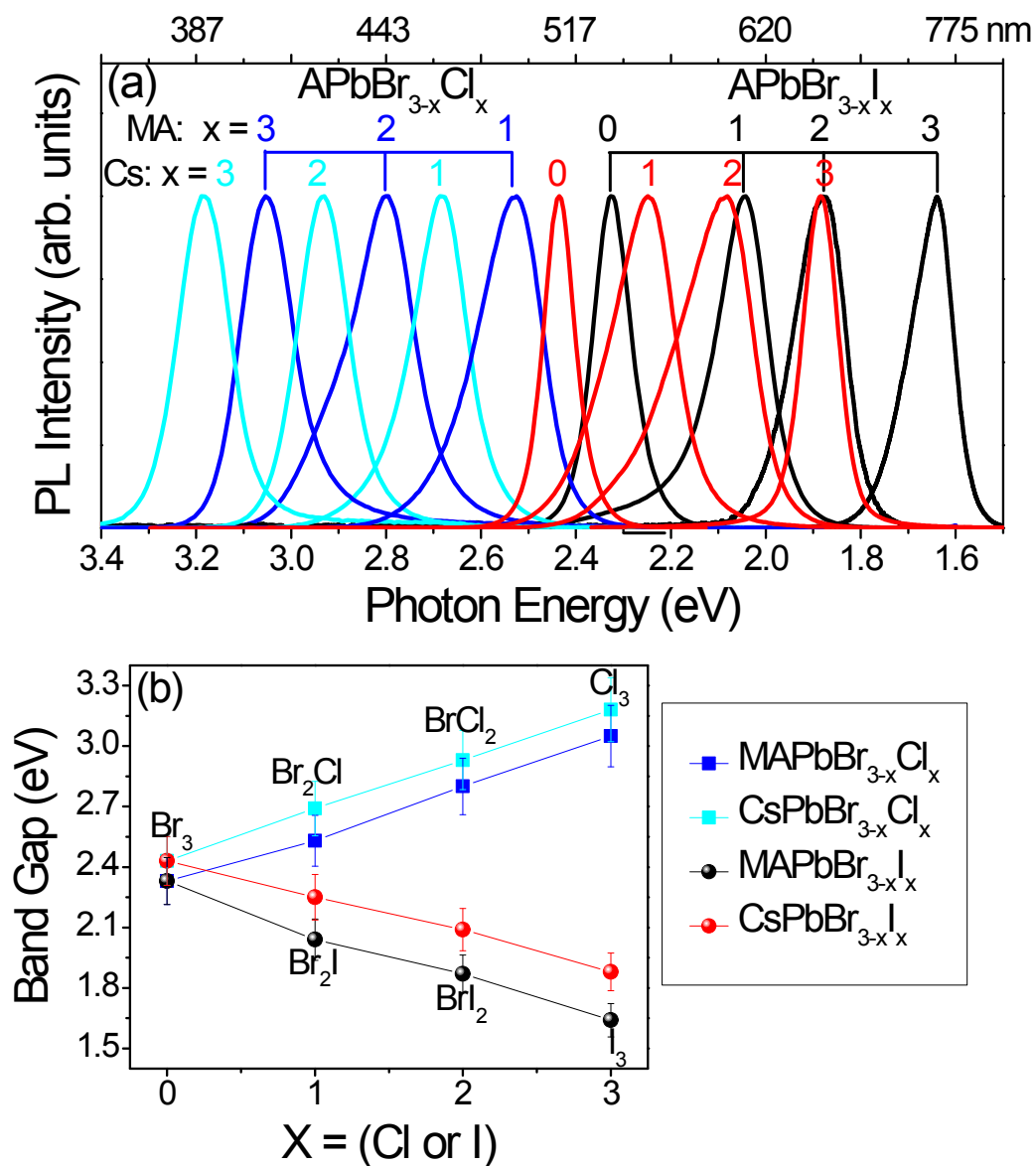


Figure S9. (a) PL spectra of MAPbBr_{3-x}Cl_x and MAPbBr_{3-x}I_x NCs at room temperature in toluene. (b) Band gaps of MAPbBr_{3-x}Cl_x and MAPbBr_{3-x}I_x as a function of x , determined from the PL spectra.

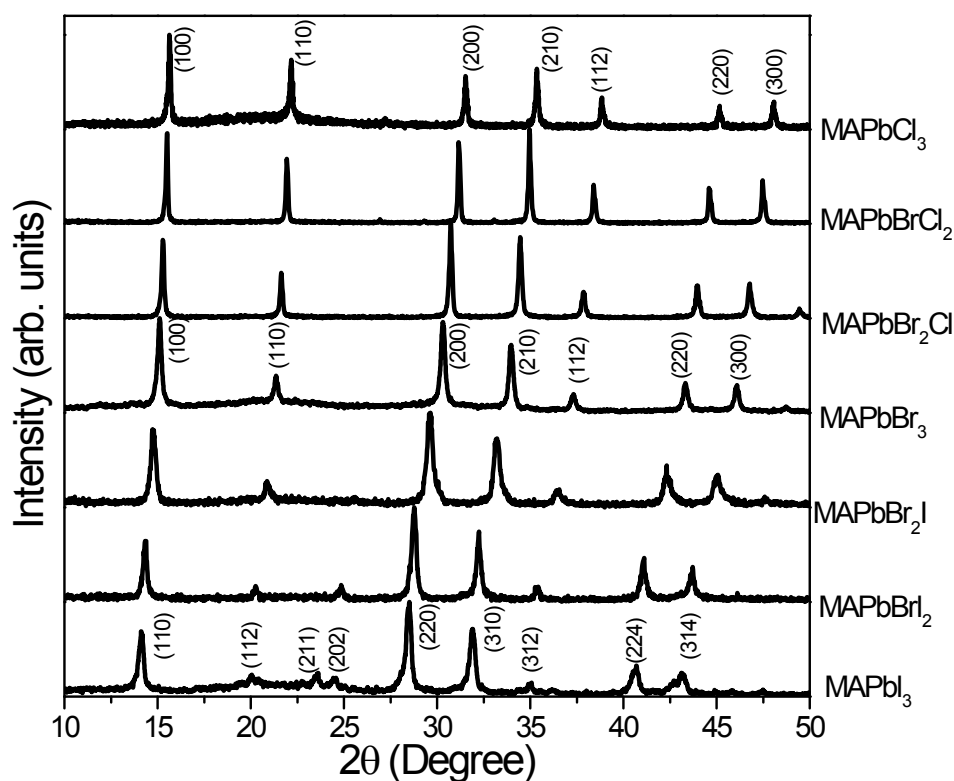
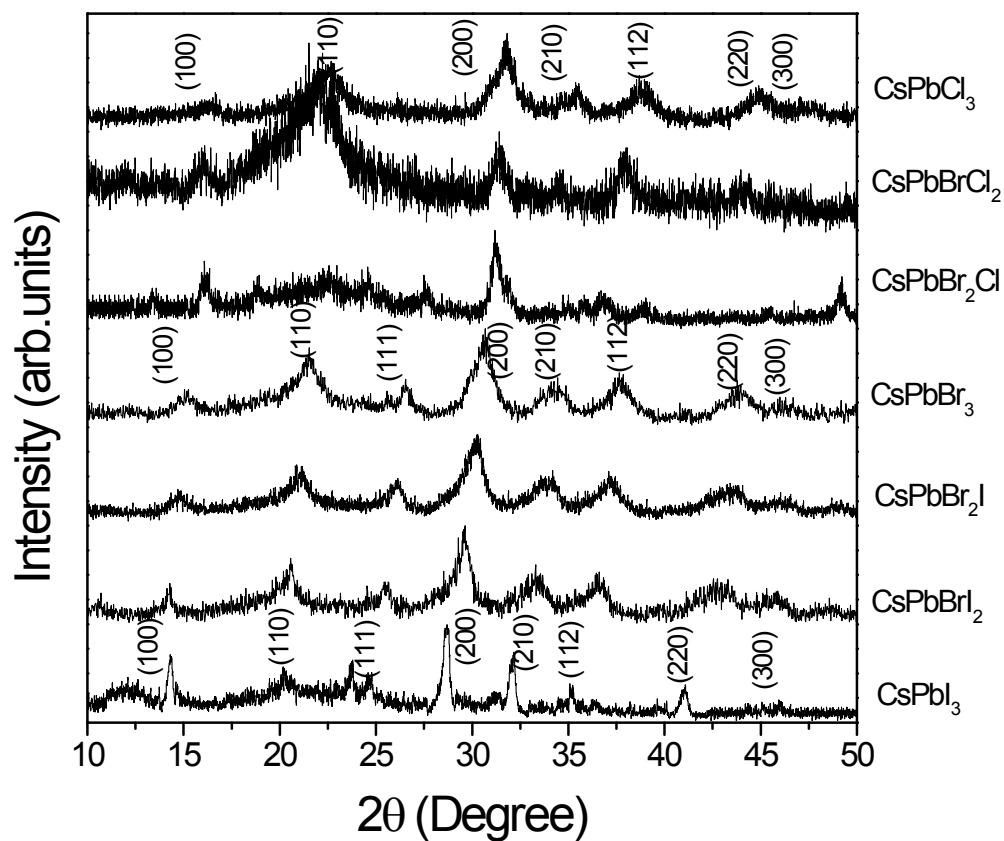


Figure S10. (a) XRD pattern of $\text{MAPbBr}_{3-x}\text{Cl}_x$ and $\text{MAPbBr}_{3-x}\text{I}_x$ NCs. The peaks of the MAPbCl_3 , MAPbBr_3 , and MAPbI_3 were indexed using the following references: $a = 5.675 \text{ \AA}$ for cubic phase MAPbCl_3 , $a = 5.90 \text{ \AA}$ for cubic phase MAPbBr_3 , and $a = 8.80 \text{ \AA}$ and $c = 12.685 \text{ \AA}$ for tetragonal phase MAPbI_3 .^{S34} As x increased, the peaks shifted from those of MAPbBr_3 to those of MAPbI_3 , with phase conversion from the cubic phase to the tetragonal phase. The XRD peaks of the $\text{MAPbBr}_{3-x}\text{Cl}_x$ NCs continuously shifted to those of cubic phase MAPbCl_3 with increasing x .



(b) XRD pattern of CsPbBr_{3-x}Cl_x and CsPbBr_{3-x}I_x NCs. The peaks of the CsPbCl₃, CsPbBr₃, and CsPbI₃ were indexed using the following references: $a = 5.605 \text{ \AA}$ for cubic phase CsPbCl₃; $a = 5.874 \text{ \AA}$ for cubic phase CsPbBr₃; $a = 6.348 \text{ \AA}$ for cubic phase CsPbI₃.^{S35,S36} As x increased, the peaks shifted from those of CsPbBr₃ to those of CsPbCl₃ or CsPbI₃.

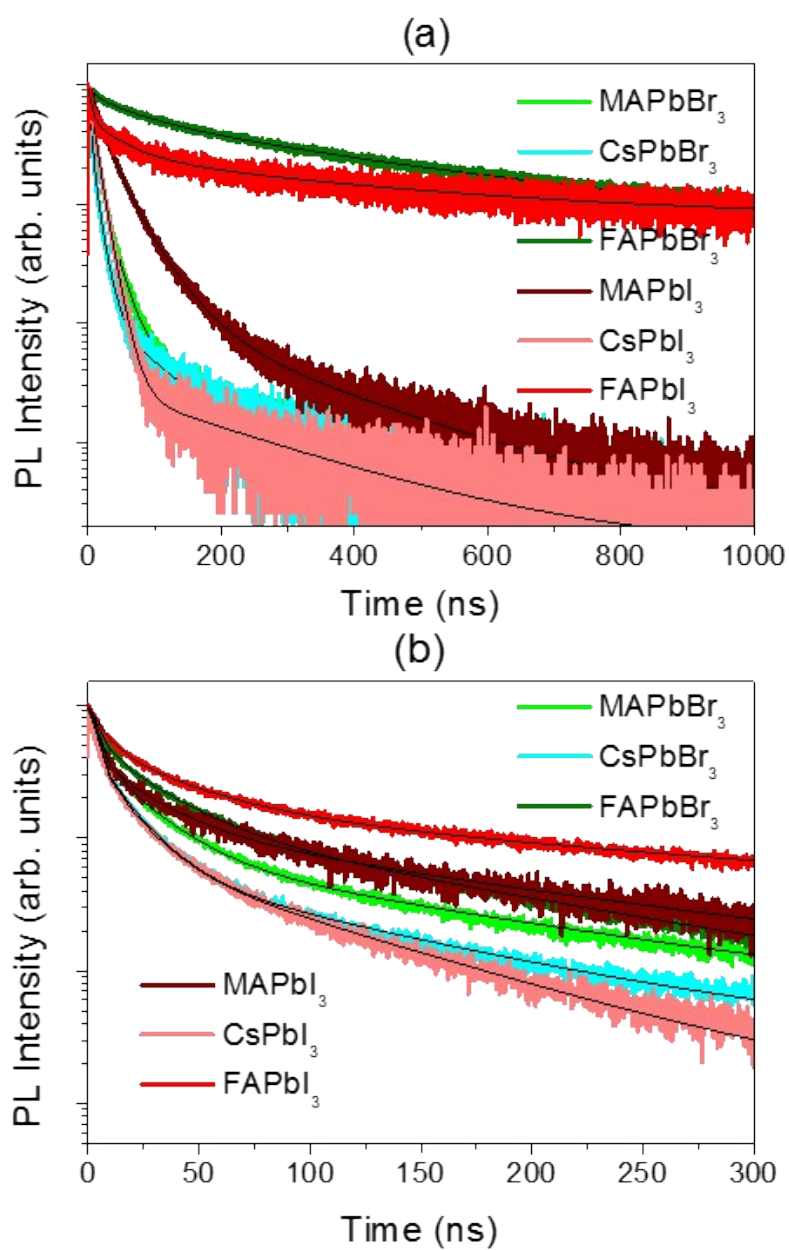


Figure S11. PL decay curves of (a) APbBr₃ and APbI₃ (A= MA, or Cs, FA) perovskite NCs (a) in toluene and (b) films measured using 355 nm excitation (intensity = 0.05 $\mu\text{J}/\text{cm}^2$). The decay curve was fitted with exponential decay function. The fitting parameters are summarized in Table S3.

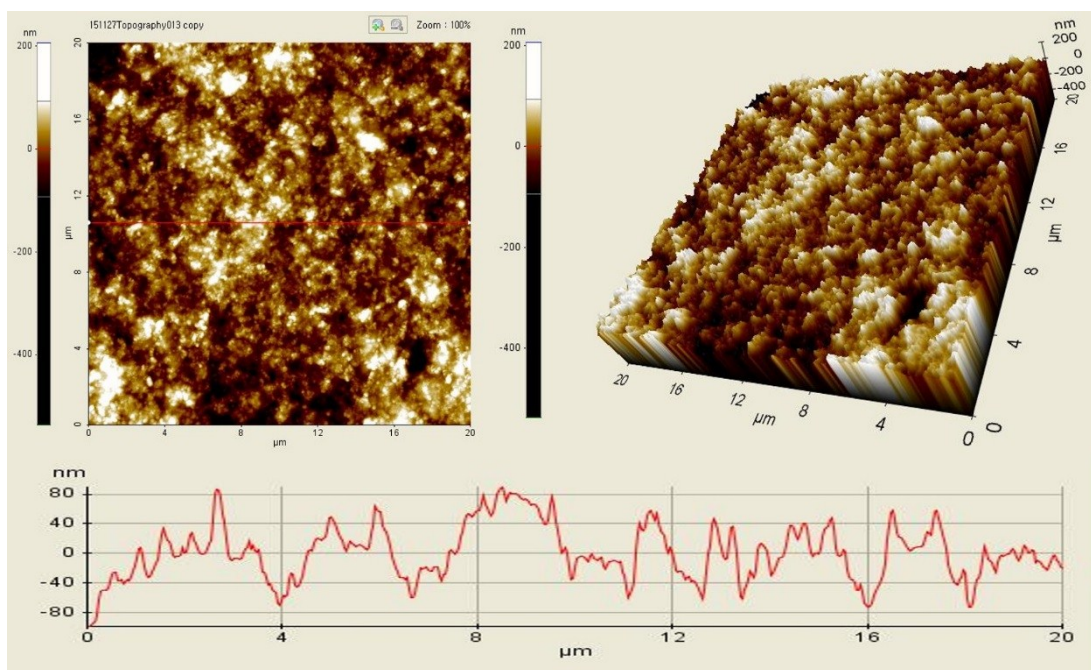


Figure S12. Atomic-force microscopy (AFM) image (with 3D image) and cross-sectional profile of the MAPbBr₃ NC film on a photodetector device. The roughness of the film was estimated to be 100 nm.

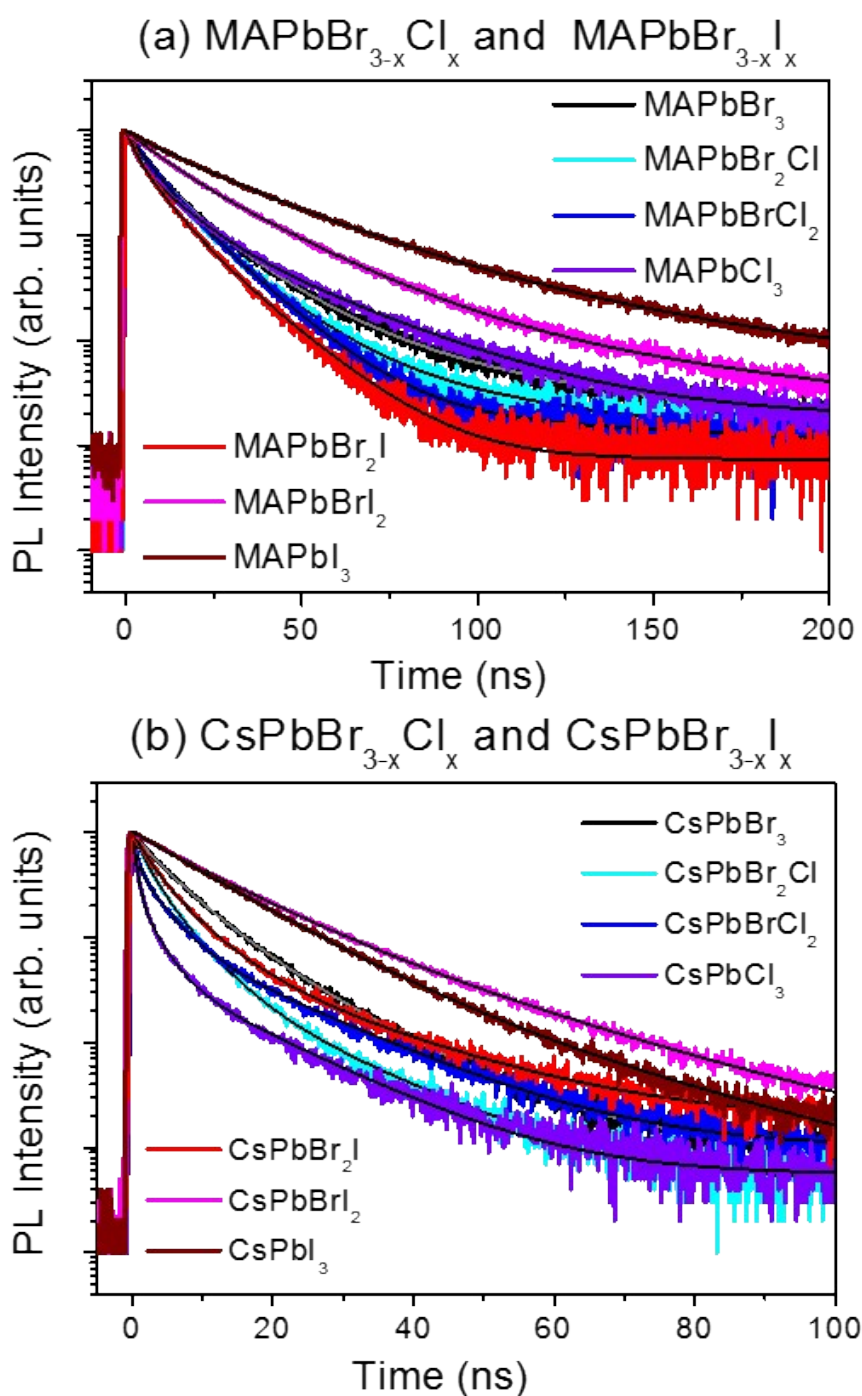


Figure S13. PL decay curves of (a) $\text{MAPbBr}_{3-x}\text{Cl}_x$ and $\text{MAPbBr}_{3-x}\text{I}_x$, and (b) $\text{CsPbBr}_{3-x}\text{Cl}_x$ and $\text{CsPbBr}_{3-x}\text{I}_x$ NCs in toluene, upon excitation at 355 nm with the lowest excitation intensity ($0.05 \mu\text{J}/\text{cm}^2$).

The decay curve was fitted with exponential decay function. The fitting parameters are summarized in Table S4. The $\langle\tau\rangle$ value of MAPbBr_3 was 13.5 ns, while those of the

MAPbBr_{3-x}Cl_x series were ~10 ns for $x = 1-3$. The $\langle\tau\rangle$ values of the MAPbBr_{3-x}I_x series were 8.1, 20.8, and 31.8 ns for $x = 1, 2,$ and $3,$ respectively. This shows an initial decrease in $\langle\tau\rangle$ when $x = 1,$ followed by an increase with increasing $x.$ The $\langle\tau\rangle$ of CsPbBr₃ is 7.4 ns. The $\langle\tau\rangle$ values of the CsPBr_{3-x}Cl_x series decreased monotonically to 1.8 ns with increasing $x.$ The $\langle\tau\rangle$ values of the CsPbBr_{3-x}I_x series were 6.8, 13.7, and 12.2 ns for $x = 1, 2,$ and $3,$ respectively. The $\langle\tau\rangle$ values of both the MA and Cs series exhibited similar composition dependences, and the longest decay times were for the I₃ and I₂Br compositions.

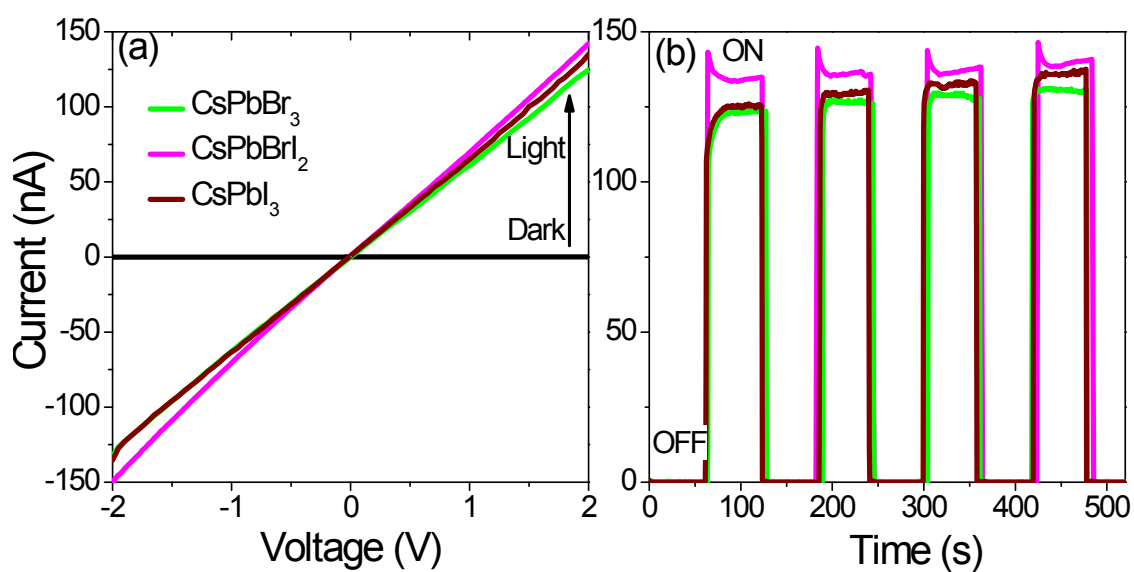


Figure S14. Photocurrent of CsPbBr₃, CsPbI₃, and CsPbBrI₂ NC films, upon excitation at 365 nm with an excitation intensity (60 mW/cm²). Similar composition dependences to the MA series were observed, with the photocurrent of the I₂Br composition being higher than for the other mixed halides.^{S37}

IV. References

- (S1) M. Grabolle, M. Spieles, V. Lesnyak, N. Gaponik, A. Eychmüller and U. Resch-Genger, *Anal. Chem.*, 2009, **81**, 6285.
- (S2) L. Dimesso, M. Dimamay, M. Hamburger and W. Jaegermann, *Chem. Mater.*, 2014, **26**, 6762.
- (S3) Y. Fang, Q. Dong, Y. Shao, Y. Yuan and J. Huang, *Nat. Photon.*, 2015, **9**, 679.
- (S4) D. Shi, V. Adinolfi, R. Comin, M. Yuan, E. Alarousu, A. Buin, Y. Chen, S. Hoogland, A. Rothenberger, K. Katsiev, Y. Losovyj, X. Zhang, P. A. Dowben, O. F. Mohammed, E. H. Sargent and O. M. Bakr, *Science*, 2015, **347**, 519.
- (S5) G. E. Eperon, S. D. Stranks, C. Menelaou, M. B. Johnston, L. M. Herz and H. J. Snaith, *Energy Environ. Sci.*, 2014, **7**, 982.
- (S6) Q. A. Akkerman, V. D'Innocenzo, S. Accornero, A. Scarpellini, A. Petrozza, M. Prato and L. Manna, *J. Am. Chem. Soc.*, 2015, **137**, 10276.
- (S7) O. N. Yunakova, V. K. Miloslavsky, E. N. Kovalenko and V. V. Kovalenko, *Low Temp. Phys.*, 2014, **40**, 690.
- (S8) C. C. Stoumpos, C. D. Malliakas, J. A. Peters, Z. Liu, M. Sebastian, J. Im, T. C. Chasapis, A. C. Wibowo, D. Y. Chung, A. J. Freeman, B. W. Wessels and M. G. Kanatzidis, *Cryst. Growth Des.*, 2013, **13**, 2722.
- (S9) F. C. Hanusch, E. Wiesenmayer, E. Mankel, A. Binek, P. Angloher, C. Fraunhofer, N. Giesbrecht, J. M. Feckl, W. Jaegermann, D. Johrendt, T. Bein and P. Docampo, *J. Phys. Chem. Lett.*, 2014, **5**, 2791.
- (S10) W. Rehman, R. L. Milot, G. E. Eperon, C. Wehrenfennig, J. L. Boland, H. J. Snaith, M. B. Johnston and L. M. Herz, *Adv. Mater.*, 2015, **27**, 7938.
- (S11) M. F. Aygüler, M. D. Weber, B. M. D. Puscher, D. D. Medina, P. Docampo and R. D. Costa, *J. Phys. Chem. C*, 2015, **119**, 12047.

- (S12) T. M. Koh, K. Fu, Y. Fang, S. Chen, T. C. Sum, N. Mathews, S. G. Mhaisalkar, P. P. Boix and T. Baikie, *J. Phys. Chem. C*, 2014, **118**, 16458.
- (S13) L. Dou, Y. (Micheal) Yang, J. You, Z. Hong, W. H. Chang, G. Li and Y. Yang, *Nat. Commun.*, 2014, **5**, 5404.
- (S14) E. Horváth, M. Spina, Z. Szekrényes, K. Kamarás, R. Gaal, D. Gachet and L. Forró, *Nano Lett.*, 2014, **14**, 6761.
- (S15) X. Hu, X. Zhang, L. Liang, J. Bao, S. Li, W. Yang and Y. Xie, *Adv. Funct. Mater.*, 2014, **24**, 7373.
- (S16) H. R. Xia, J. Li, W. T. Sun and L. M. Peng, *Chem. Commun.*, 2014, **50**, 13695.
- (S17) Y. Lee, J. Kwon, E. Hwang, C. H. Ra, W. J. Yoo, J. H. Ahn, J. H. Park and J. H. Cho, *Adv. Mater.*, 2015, **27**, 41.
- (S18) R. Dong, Y. Fang, J. Chae, J. Dai, Z. Xiao, Q. Dong, Y. Yuan, A. Centrone, X. C. Zeng and J. Huang, *Adv. Mater.*, 2015, **27**, 1912.
- (S19) Y. Fang and J. Huang, *Adv. Mater.*, 2015, **27**, 2804.
- (S20) S. Zhuo, J. Zhang, Y. Shi, Y. Huang and B. Zhang, *Angew. Chem. Int. Ed.*, 2015, **54**, 5693.
- (S21) H. Deng, X. Yang, D. Dong, B. Li, D. Yang, S. Yuan, K. Qiao, Y. B. Cheng, J. Tang and H. Song, *Nano Lett.*, 2015, **15**, 7963.
- (S22) M. I. Saidaminov, V. Adinolfi, R. Comin, A. L. Abdelhady, W. Peng, I. Dursun, M. Yuan, S. Hoogland, E. H. Sargent and O. M. Bakr, *Nat. Commun.*, 2015, **6**, 8724.
- (S23) S. Chen, C. Teng, M. Zhang, Y. Li, D. Xie and G. Shi, *Adv. Mater.*, 2016, **28**, 5969.
- (S24) V. Adinolfi, O. Ouellette, M. I. Saidaminov, G. Walters, A. L. Abdelhady, O. M. Bakr, and E. H. Sargent, *Adv. Mater.*, 2016, **28**, 7264.
- (S25) D. -H. Kang, S. R. Pae, J. Shim, G. Yoo, J. Jeon, J. W. Leem, J. S. Yu, S. Lee, B. Shin and J. -H. Park, *Adv. Mater.*, 2016, **28**, 7799.

- (S26) M. I. Saidaminov, Md. A. Haque, M. Savoie, A. L. Abdelhady, N. Cho, I. Dursun, U. Buttner, E. Alarousu, T. Wu and O. M. Bakr, *Adv. Mater.* 2016, **28**, 8144.
- (S27) P. Ramasamy, D. -H. Lim, B. Kim, S. -H. Lee, M. -S. Lee and J. -S. Lee, *Chem. Commun.*, 2016, **52**, 2067.
- (S28) F. Zhang, H. Zhong, C. Chen, X. Wu, X. Hu, H. Huang, J. Han, B. Zou and Y. Dong, *ACS Nano*, 2015, **9**, 4533.
- (S29) Y. Tong, E. Bladt, M. F. Aygüler, A. Manzi, K. Z. Milowska, V. A. Hintermayr, P. Docampo, S. Bals, A. S. Urban, L. Polavarapu and J. Feldmann, *Angew. Chem. Int. Ed.*, 2016, DOI: 10.1002/anie.201605909.
- (S30) H. Huang, A. S. Susha, S. V. Kershaw, T. F. Hung and A. L. Rogach, *Adv. Sci.*, 2015, **2**, 1500194.
- (S31) S. Gonzalez-Carrero, R. E. Galian and J. Pérez-Prieto, *Opt. Express*, 2016, **24**, A285.
- (S32) C. -H. Lu, J. Hu, W. Y. Shih and W. -H. Shih, *J. Colloid Interface Sci.*, 2016, **484**, 17.
- (S33) L. Protesescu, S. Yakunin, M. I. Bodnarchuk, F. Bertolotti, N. Masciocchi, A. Guagliardi and M. V. Kovalenko, *J. Am. Chem. Soc.*, 2016, DOI: 10.1021/jacs.6b08900.
- (S34) A. Poglitsch and D. Weber, *J. Chem. Phys.*, 1987, **87**, 6373.
- (S35) C. K. Møller, *Nature*, 1958, **182**, 1436.
- (S36) L. Protesescu, S. Yakunin, M. I. Bodnarchuk, F. Krieg, R. Caputo, C. H. Hendon, R. X. Yang, A. Walsh and M. V. Kovalenko, *Nano Lett.*, 2015, **15**, 3692.
- (S37) D. M. Jang, K. Park, D. H. Kim, J. Park, F. Shojaei, H. S. Kang, J. -P. Ahn, J. W. Lee and J. K. Song, *Nano Lett.*, 2015, **15**, 5191.